JOURNAL OF COMPUTATIONAL PHYSICS 36, 35–54 (1980)

Evolution of Flux-Conserving Tokamak Equilibria with Preprogrammed Cross Sections*

J. A. HOLMES

Computer Sciences Division, Oak Ridge National Laboratory, Oak Ridge, Tennessee 37830

Y.-K. M. PENG

Fusion Energy Division, Oak Ridge National Laboratory, Oak Ridge, Tennessee 37830

AND

S. J. LYNCH

Computer Sciences Division, Oak Ridge National Laboratory, Oak Ridge, Tennessee 37830

Received February 28, 1979; revised June 6, 1979

The evolution of MHD equilibria toward high β is modeled by magnetic flux conservation with a given $q(\psi)$ and by single fluid particle and energy balances which determine $p(\psi, t)$. These one-dimensional flux surface averaged equations, written with magnetic flux ψ as the independent variable, are coupled to the two-dimensional MHD equilibrium equation through ψ, $p(\psi, t)$, and $q(\psi)$. The location and evolution of the plasma cross section boundary are precisely specified through the use of a fixed boundary equilibrium technique. In moving boundary studies (e.g., plasma compression) the resulting system of equations is advanced in time from an initial state by a procedure which utilizes two nested predictor–corrector loops together with an implicit time-stepping technique. The inner predictor–corrector loop advances the transport equations subject to a given equilibrium configuration while the outer loop evolves the equilibrium. For fixed plasma boundaries this procedure is modified for greater computational speed. These techniques provide satisfactory numerical convergence together with complete consistency between the coupled one-dimensional system of equations and the two-dimensional equilibrium. This method can be applied to the study of equilibrium evolution involving dramatic changes of plasma position, shape, and profiles while prescribing the evolution of the plasma boundary. As such, it can serve as a useful tool in the design of poloidal field systems or as a source of equilibria in high-β MHD stability studies. As an example, the compressional scaling laws of Furth and Yoshikawa are found to be modified for small aspect ratio.

* Research sponsored by the Office of Fusion Energy, U.S. Department of Energy under contract W-7405-eng-26 with the Union Carbide Corporation.

0021-9991/80/070035-20$02.00/0

1. INTRODUCTION

The study of two-dimensional tokamak transport has enjoyed considerable attention recently. This attention is due in part to some recent calculations of high-β equilibria in flux-conserving tokamaks (FCT) [1, 2] and to experiments with non-circular cross sections [3–5]. A common approach to two-dimensional transport involves the time integration of one-dimensional particle balance, energy balance, and flux diffusion equations which are averages over the flux surfaces [6–11]. These equations are coupled to the two-dimensional MHD equilibrium equation through the safety factor and pressure profiles, and through several geometric coefficients which depend upon the flux surface configuration. The evolving safety factor and pressure profiles are used as input functions in continually recalculating the equilibrium, and the resulting geometric factors enter the one-dimensional transport equations as coefficients.

A prevailing emphasis in these calculations has been to include the effects of the two-dimensional force balance in assessing the relevancy of various transport processes for the interpretation and extrapolation of experimental results. The physical assumptions and mathematical methods used in these calculations vary with the specific applications being considered. Our emphasis is different in that we use flux surface averaged transport as a tool to study equilibrium evolution. With proper models for transport processes, the resulting profiles are expected to be more realistic than the arbitrarily prescribed functions used in typical equilibrium studies.

The equilibrium modules in the existing studies generally use computationally fast free boundary techniques. However, relatively little dynamic control of the plasma cross section is incorporated, and significant and arbitrary alterations in plasma shape and position usually result during large changes in plasma β. An exception is the work of Byrne and Klein [11] in which a constant plasma cross section boundary is maintained with the use of orthogonal flux coordinates. The use of orthogonal flux coordinates makes it inconvenient for us to study the equilibrium evolution in detail.

In the case of flux-conserving equilibria, it has been demonstrated [2] that, during rapid plasma heating, a change of a few percent in the plasma minor radius will result in a skin current comparable to the plasma current. Such a skin current, as it diffuses through the plasma periphery, is expected to have a strong effect on the subsequent plasma confinement, stability, and evolution [12]. It is, therefore, desirable to exercise relatively precise control of the plasma shape and position in order to avoid generating the skin current and to properly simulate the plasma equilibrium evolution in non-circular high-β tokamak experiments [4, 5].

The uncertainties in equilibrium cross section can be avoided by a time-dependent prescription of the plasma cross section and position that is independent of the transport calculations. The "fixed boundary" approach with arbitrarily prescribed cross section [13] is used for this purpose. The resulting equilibria can then be used as input for high-β MHD stability calculations, or to provide information on the evolving external poloidal fields required, which may then be used to determine the required current evolution of the poloidal field coils [14]. The plasma shape and

position control requirements are expected to be most severe during rapid heating (by neutral beam or adiabatic compression). Because the flux is well conserved in this situation, we now study the case where the q-profile is unchanged.

Our emphasis is on developing numerical schemes for studying the evolution of noncircular MHD equilibria. For convenience, only a one-fluid approximation to the particle and energy balance equations will be used in this work. Profiles of diffusion and conduction coefficients consistent with experimental observations [15, 16] are used to give realistic pressure profiles. These restrictions to a one-fluid flux-conserving plasma are not crucial to the numerical approach used. More sophisticated transport models and magnetic flux diffusion can easily be incorporated when the need arises.

In the following sections, we briefly indicate the physics models and equations involved in this work (Section 2), then discuss in detail the numerical procedures employed (Section 3) and some results demonstrating the utility of this approach (Section 4).

2. Physics Models and Equations

2.1. *MHD Equilibrium*

The instantaneous equilibrium state of an axisymmetric toroidal plasma is described by the Grad–Shafranov equation

$$\begin{aligned} \Delta^*\psi &= R\frac{\partial}{\partial R}\left(\frac{1}{R}\frac{\partial\psi}{\partial R}\right) + \frac{\partial^2\psi}{\partial Z^2} \\ &= -4\pi R^2 p'(\psi) - FF'(\psi), \end{aligned} \tag{1}$$

in which

$$\psi(R, Z) = RA_\phi \tag{2}$$

is the poloidal magnetic flux function, p is the pressure,

$$F(\psi) = RB_\phi \tag{3}$$

is the toroidal magnetic flux function, and the prime denotes differentiation with respect to ψ. In terms of ψ and F, the magnetic field is given by

$$\mathbf{B} = \frac{1}{R}\nabla\psi \times \hat{\phi} + \frac{F}{R}\hat{\phi}, \tag{4}$$

where $\hat{\phi}$ is the unit vector in the toroidal direction.

2.2. *Flux Conservation*

Magnetic flux conservation requires that the safety factor

$$q(\psi) = (1/4\pi^2)\, FV'\langle R^{-2}\rangle \tag{5}$$

and the total poloidal flux $\psi_{\text{edge}} - \psi_0$ remain fixed as the plasma evolves in time. The $\langle\ \rangle$ notation in Eq. (5) denotes an average [17] over surfaces of constant ψ, and $V(\psi)$ denotes the volume contained within a flux surface ψ. Equation (1) can be averaged over flux surfaces and combined with Eqs. (4) and (5) in various ways to yield several equations. We use two of these in the numerical procedure to obtain an equilibrium of given safety factor (see Section 3):

$$\frac{d}{dV}\left(\left\langle\frac{|\nabla V|^2}{R^2}\right\rangle\frac{d\psi}{dV}\right) + (2\pi)^4 q(\psi)\frac{d}{dV}\left[\frac{q(\psi)}{\langle R^{-2}\rangle}\frac{d\psi}{dV}\right] = -4\pi p'(\psi) \tag{6}$$

and

$$\frac{dF^2}{d\psi}\left[\frac{\langle R^{-2}\rangle}{2} + \frac{1}{2}\left\langle\frac{|\nabla V|^2}{R^2}\right\rangle\left(\frac{\langle R^{-2}\rangle}{4\pi^2 q}\right)^2\right] + F^2\left[\frac{\langle R^{-2}\rangle}{4\pi^2 q}\frac{d}{d\psi}\left(\left\langle\frac{|\nabla V|^2}{R^2}\right\rangle\frac{\langle R^{-2}\rangle}{4\pi^2 q}\right)\right] = -4\pi p'(\psi). \tag{7}$$

These equations are similar to those proposed by Grad and co-workers [18].

2.3. *Transport Equations*

Single-fluid particle and energy balance equations are assumed for convenience. They can be averaged over each flux surface to obtain the following one-dimensional equations in which ψ is the independent variable:

$$\frac{\partial}{\partial t}(nV') = (n'V'\langle DR^2 B_p{}^2\rangle)' + V'(\langle S_{\text{inj}}\rangle + \langle S_{\text{fuel}}\rangle), \tag{8}$$

$$\frac{\partial}{\partial t}(pV'^{5/3}) = \left(pV'^{5/3}\frac{n'}{n}\langle DR^2 B_p{}^2\rangle\right)' + \frac{2}{3}pV'^{5/3}\left(\frac{n'}{n}\langle DR^2 B_p{}^2\rangle\right)' + \frac{2}{3}V'^{2/3}\left[\left(\frac{p}{n}\right)' nV'\langle\chi R^2 B_p{}^2\rangle\right]' + \frac{2}{3}V'^{5/3}(\langle\eta J_\phi{}^2\rangle + \langle H_\alpha\rangle + \langle H_{\text{inj}}\rangle), \tag{9}$$

where $n(\psi, t)$ and $p(\psi, t)$ are the particle density and pressure, respectively; D and χ are the particle and heat conduction coefficients, respectively; $B_p{}^2$ is the square of the poloidal **B** field; η is the plasma resistivity; $\langle S_{\text{inj}}\rangle$ and $\langle S_{\text{fuel}}\rangle$ are the flux surface averaged injection and fueling particle sources, respectively; and $\langle\eta J_\phi{}^2\rangle$, $\langle H_\alpha\rangle$, and $\langle H_{\text{inj}}\rangle$ are the flux surface averaged ohmic, nuclear alpha, and injection heating sources, respectively. The ideal gas law $p = nkT$ is assumed.

2.4. *Transport Coefficients and Sources*

Equations (1), (5), (8), and (9) comprise our present approach to the time evolution of MHD equilibria, subject to particle and temperature diffusion and to various

particle and energy source terms. We now describe the simple models of the transport coefficients and source term.

The plasma resistivity is chosen to be the Spitzer resistivity. The heat conduction coefficient χ is taken to consist of anomalous electron plus neoclassical ion contributions

$$\chi = (\chi_e + \chi_i)/2. \tag{10}$$

The anomalous electron term is given by

$$\chi_e = 5 * 10^{17}/n_e \frac{\text{cm}^2}{\text{sec}}$$

$$= 1 * 10^{18}/n \frac{\text{cm}^2}{\text{sec}}, \tag{11}$$

where the electron density is in particles/cm^3. The formulation for the neoclassical ion conductivity is taken from Hinton and Hazeltine [19]. The particle diffusion coefficient is taken to be

$$D = \chi_e/5 = 1 * 10^{17}/n_e \frac{\text{cm}^2}{\text{sec}}$$

$$= 2 * 10^{17}/n \frac{\text{cm}^2}{\text{sec}}. \tag{12}$$

These diffusion coefficients are in good agreement with experimental observations [20] of low-density ohmically heated tokamak discharges for reasonable choices of $p(\psi)$, $n(\psi)$, and $q(\psi)$. These simple diffusion coefficients are considered adequate for our purpose since the physical mechanisms for heat conduction and particle transport in tokamaks are yet to be fully understood [15, 16]. We have included deuterium–tritium (D–T) burning as an energy source to be used when the effects of α-particle heating are studied. In this case the deuterium and tritium particle densities are each assumed to be equal to one-fourth the total particle (electrons and ions) density. Reaction rate formulas for D–T burning were taken from the fitting formulas of Fowler, *et al.* [21]. When particle fueling is desired, the particle fueling source is assumed to be uniform to a chosen depth in the plasma beyond which it drops exponentially at a chosen rate. The neutral injection energy and particle source terms are calculated using the modified Monte Carlo injection package, NFREYA [22].

3. Numerical Procedures

3.1. *Specification of the Problem*

The evolution of MHD equilibria subject to magnetic flux conservation, to particle and energy transport, and to the motion of the plasma cross section boundary is determined by Eqs. (5), (8), and (9) coupled to the equilibrium Eq. (1). The transport

coefficients and source terms described above may all be considered as functions of ψ (through flux surface averaging) and t, which can be evaluated at the time of each step.

3.2. *Initial-Value Problem*

The system of equations to be studied presents an initial-value problem; i.e., given the initial state of the plasma and prescriptions for calculating the transport coefficients, source terms, and evolution of the plasma cross section boundary, the subsequent behavior of the plasma can be calculated. The initial state requires the specification of the dimensions and cross-sectional shape of the plasma; the initial pressure, density, and toroidal flux function [$p(\psi)$, $n(\psi)$, and $F(\psi)$, respectively]; and the initial equilibrium $\psi(R, Z)$. The total poloidal flux $\psi_{\text{edge}} - \psi_0$ and the safety factor $q(\psi)$ can then be evaluated. The specification of $\langle S_{\text{inj}} \rangle(\psi)$, $\langle S_{\text{fuel}} \rangle(\psi)$, $\langle H_{\text{inj}} \rangle(\psi)$, and the cross section boundary as functions of t then complete the input required to study the evolution of the plasma.

3.3. *Fixed Boundary Equilibrium Procedure*

Before considering the full time-stepping procedure, we will describe the solution of the Grad–Shafranov equation (1) for given $p(\psi, t)$, $q(\psi)$, $\psi_{\text{edge}} - \psi_0$, and $F(\psi_{\text{edge}}, t)$. We separate this problem into two parts: an inner two-dimensional part in which Eq. (1) is inverted for a given $F(\psi)$ and an outer one-dimensional part in which $F(\psi)$ and the plasma minor radius a are iterated to obtain the desired $q(\psi)$ and $\psi_{\text{edge}} - \psi_0$. This entire procedure is independent of the flux conservation assumption since $q(\psi)$ and $\psi_{\text{edge}} - \psi_0$ can be functions of time without affecting the procedure, which is carried out at a point in time. In order to control closely the evolution of the plasma cross section boundary, we use a fixed-boundary technique to invert Eq. (1). Once a rectangular coordinate grid in R and Z is chosen, the boundary of the plasma is specified to lie anywhere within the chosen coordinate grid. We allow for circular, elliptical, or D-shaped plasmas. The desired boundary condition on ψ is maintained by specifying ψ at grid points which are exterior but adjacent to the boundary ("ghost points"). We have chosen a conducting wall boundary condition of

$$\psi_{\text{edge}} = 0. \tag{13}$$

Equation (1) is then solved inside the plasma boundary by an iterative procedure, with the ghost points and their ψ values forming the numerical boundary of the solution. Periodically, as the procedure converges, the ghost point values of ψ are changed to maintain the desired boundary condition. We use the method of successive overrelaxations (SOR) in order to invert Eq. (1). Because of the simple transport model assumed, much of the computing time is spent in the equilibrium portion of the program. Hence, it is important to use an efficient procedure to carry out the equilibrium. In detail, our procedure is the following [23] (see Fig. 1):

(a) Let superscript k denote a source iteration step number, initially $k = 0$. Establish an initial guess $\psi^{(0)}(R, Z)$ for the poloidal flux function. During the transport

calculation, the solution of the previous equilibrium is used as the initial guess. When no previous solution exists, $\psi^{(0)}$ is taken to be quadratic in form with a minimum at the major radius midplane $(R, Z) = (R_0, 0)$. In this case $\psi^{(0)}$ is extrapolated to the ghost points using the conducting wall boundary condition.

(b) Calculate the right-hand side of Eq. (1) as a function $s^{(0)}(R, Z)$ using the given functions $p(\psi)$ and $F^2(\psi)$ together with $\psi^{(0)}$.

(c) Invert the linear equation $\Delta^*\psi^{(k+1)} = s^{(k)}(R, Z)$ by SOR to obtain $\psi^{(k+1)}$. Extrapolate $\psi^{(k+1)}$ to the ghost points using the conducting wall boundary condition.

(d) Calculate $s^{(k+1)}(R, Z)$, the right-hand side of Eq. (1), using $\psi^{(k+1)}$.

(e) Compare $s^{(k+1)}(R, Z)$ to $s^{(k)}(R, Z)$. If converged, continue to step *f*. Otherwise, set $k \rightarrow k + 1$ and return to step (c).

(f) The procedure has converged to the new equilibrium solution $\psi(R, Z) = \psi^{(k+1)}(R, Z)$.

The rate of convergence of the procedure described above depends in two ways upon the initial guess for ψ. First, a poor initial guess for ψ results in a larger number of source function iterations than does a good initial guess. Also, a poor initial guess

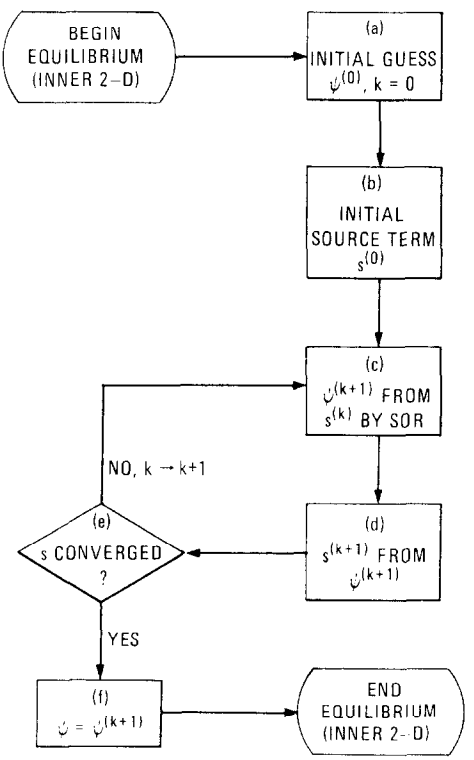

FIG. 1. Flowchart o the inner two-dimensional equilibrium numerical procedure described in Section 3.

for ψ can lead, during the first few source function iterations, to a greater number of SOR iterations in step (c), which are necessitated by significant changes in the source function. In choosing an initial guess for $\psi(R, Z)$, we make use of the fact that ψ changes slowly both in time and in successive iterations of F and a (see below). Hence, the previous equilibrium solution at the corresponding grid points provides a good initial guess for ψ, even in the case of compression, where the location and spacing of the grid points, but not their number, change in time.

It is well known that the SOR technique may converge for relaxation factors between 0 and 2. For 32×26, 40×32, and 154×126 grid sizes, we have found the optimal values for the relaxation factors to be 1.85, 1.88, and 1.97, respectively. Hence, the magnitude of the relaxation factor increases with the number of points in the two-dimensional grid. We have also found it necessary to relax the source function s before proceeding from step (e) to step (c) in the iteration. We have found the optimal value of this relaxation factor to be 0.75, so that $s^{(k-1)} \rightarrow 0.75s^{(k-1)} + 0.25s^{(k)}$ after the completion of step (e).

Although Eq. (1) is inverted only linearly, the iteration procedure described above allows the solution of the full nonlinear problem through reevaluation of the source function $s^{(k)}(R, Z)$. An alternative method of calculating fixed boundary equilibria involves updating the source function with each SOR iteration, so that the SOR residual in ψ and the source function residual in s converge simultaneously. Although this method requires fewer SOR iterations than the present technique, each iteration is accompanied by an update of the source function over the entire two-dimensional grid. In order to minimize the required number of source function iterations, we have chosen to converge the SOR solution for a given source function, as in step (c) above, before iterating the source function. By this method the number of source function iterations is typically reduced by more than a factor of 2, although this gain is partially offset by an increase in the number of SOR iterations. On a variety of cases comparing the timing of the two techniques, the adopted procedure runs up to 50% faster on a CDC-7600 computer than the other method.

This procedure converges to 10^{-4} in the source function residual in 5–20 iterations, depending on the initial guess, for an (R, Z) grid of 32×26 points in the upper half plane. The linear SOR part of the equilibrium solver converges to 10^{-5} residual in ψ in 5–50 iterations. Typically, 30–50 SOR iterations are required for the linear problem during the early nonlinear steps when the source function residual is large, but, as the source function residual decreases, fewer SOR iterations are required to solve the linear problem.

The outer part of the equilibrium procedure iterates $F(\psi)$ and the plasma minor radius a in order to obtain the desired $q(\psi)$ and $\psi_{\text{edge}} - \psi_0$. Basically, the safety factor q is sensitive to the iteration of F, while $\psi_{\text{edge}} - \psi_0$ is dependent upon a for given $F(\psi_{\text{edge}})$. An alternative possibility would be to iterate $F(\psi_{\text{edge}})$ for a given minor radius a. Letting superscript k denote the iteration index, we follow the scheme below (see Fig. 2):

(a) Make an initial guess $F^{(0)}(\psi)$ for the toroidal flux and $a^{(0)}$ for the minor radius.

Typically we set $F^{(0)}$ to the values at the previous time step and $a^{(0)}$ to some prescribed value.

(b) Solve $\Delta^*\psi^{(k)} = -4\pi R^2 p' - F^{(k)}F^{(k)'}$ by the fixed boundary equilibrium procedure discussed above. Evaluate $(\psi_{\text{edge}} - \psi_0)^{(k)}$.

(c) Evaluate $q^{(k)}(\psi) = (1/4\pi^2)\, F^{(k)}V^{(k)'}\langle R^{-2}\rangle^{(k)}$ using $\psi^{(k)}(R, Z)$ to determine flux surfaces of constant ψ and, hence, $V^{(k)}(\psi)$ and $\langle R^{-2}\rangle^{(k)}$.

(d) Compare $q^{(k)}(\psi)$ to $q(\psi)$ and $(\psi_{\text{edge}} - \psi_0)^{(k)}$ to $\psi_{\text{edge}} - \psi_0$. If converged, continue to step (e). Otherwise, apply the method described below to obtain $F^{(k+1)}(\psi)$ and $a^{(k+1)}$, set $k \to k + 1$, and return to step (b).

(e) The solution has converged with $F(\psi) = F^{(k)}(\psi)$, $a = a^{(k)}$, and $\psi(R, Z) = \psi^{(k)}(R, Z)$.

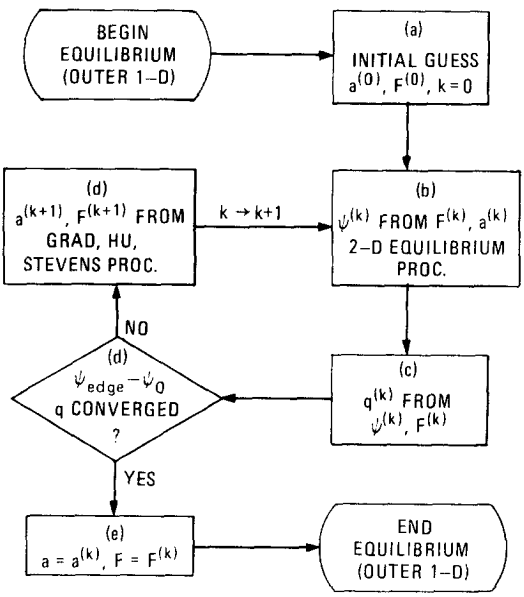

FIG. 2. Flowchart of the outer one-dimensional equilibrium numerical procedure described in Section 3.

The values of $a^{(0)}$ and $a^{(1)}$ are obtained by prescribed guesses. Thereafter $a^{(k+1)}$ is obtained from $a^{(k)}$, $a^{(k-1)}$, $(\psi_{\text{edge}} - \psi_0)^{(k)}$, $(\psi_{\text{edge}} - \psi_0)^{(k-1)}$, and $\psi_{\text{edge}} - \psi_0$ using the secant method. Convergence of $\psi_{\text{edge}} - \psi_0$ to 10^{-3} is obtained in two or three iterations.

The convergence of the outer part of the equilibrium procedure depends in two ways upon the initial guess for $F(\psi)$. More iterations of F will be required for a poor initial guess than for a good initial guess. In addition, the fixed boundary equilibrium procedure used in step (b) will require more iterations for a poor initial guess of F, parti-

cularly during the early F iterations, in which significant changes in F cause the initial guess for ψ (the equilibrium solution from the previous F iteration) to be inaccurate. Because the variation of the toroidal flux function $F(\psi)$ in time and in successive transport predictor–corrector iterations is slow, the use of the previous $F(\psi)$ is a good initial guess in step (a). This part of the equilibrium procedure is not used to obtain the plasma state at the initial time for which $F(\psi)$ and a are specified and $q(\psi)$ and $\psi_{\text{edge}} - \psi_0$ are calculated as results.

In order to determine the surfaces of constant ψ, which are required for the calculation of average quantities in both the outer equilibrium and transport procedures, linear interpolation of $\psi(R, Z)$ between adjacent points in both the horizontal and vertical directions of the two-dimensional grid is used. For each value of ψ the set of points so determined constitutes the flux surface on which the averaged quantities are calculated.

In present calculations we maintain a constant value of F at the plasma edge:

$$F(\psi_{\text{edge}}, t) = F_{\text{edge}} = \text{constant}. \tag{14}$$

The iteration procedure for F contained in step (d) must fulfill this condition. For minor radius compressions at fixed major radius, which are not discussed here, $F(\psi_{\text{edge}}, t)$ must be an increasing function of time. Also, with the adopted method, we found it necessary to introduce a relaxation factor into the iteration of F. The optimum value of this factor is 0.5, so that $F^{2(k+1)} \to 0.5F^{2(k+1)} + 0.5F^{2(k)}$ between the completion of step (d) and the return to step (b).

The convergence of the safety factor profile depends on the technique used to iterate F in step (d) [2]. We use a method similar to that described by Grad, *et al.* [18]. This method utilizes the two-flux surface averaged forms of the Grad–Shafranov equation given by Eqs. (6) and (7). In Eq. (6), ψ is regarded as a function of the flux surface volume V, as are $\langle |\nabla V|^2/R^2 \rangle$ and $\langle R^{-2} \rangle$. However, q and p' are regarded as functions of ψ. Equation (7) is an equation for F^2 with all quantities regarded as functions of ψ. The method used in step (d) consists in the following:

(1) Solve Eq. (6) for $\psi(V)$ using $\langle |\nabla V|^2/R^2 \rangle^{(k)}$ and $\langle R^{-2} \rangle^{(k)}$. This can be done on an equally spaced volume grid using SOR. The boundary values of ψ, namely ψ at the magnetic axis and at the plasma boundary, must be specified. When all quantities are interpolated back into an equally spaced ψ grid, the net effect of this step is to alter the values of ψ assigned to specific flux surfaces, but not the geometry of the flux surfaces or the functions $p'(\psi)$ or $q(\psi)$. Hence, step (1) simply alters the functions $V(\psi)$,

[redacted]

from the reparameterization in step (1). $F^{2(k+1)}(\psi)$ could also be obtained from Eq. (5) using the new values of V' and $\langle R^{-2} \rangle$. However, the integration procedure associated with Eq. (7) leads to smoother values of $F^{2(k+1)}(\psi)$ than does the direct evaluation of Eq. (5). This is done by direct integration on an equally spaced ψ grid. The boundary condition is chosen to maintain $F(\psi_{\text{edge}}, t)$ constant.

For typical cases using grid sizes of 31 points in both ψ and V, we find that the outer part of the equilibrium procedure converges to within 2×10^{-3} of the desired safety factor in 5–10 iterations, depending on the initial guess for $F(\psi)$.

3.4. *Transport Equations*: *Time Stepping*

In this section we shall describe a method of advancing the transport equations (8) and (9) which was developed for compressional studies in which the plasma cross section boundary is prescribed as a function of time. This method can be modified to gain increased computational speed for studies having constant plasma boundary.

Equations (8) and (9) are written in adiabatic form, featuring time derivatives of nV' and $pV'^{5/3}$, respectively. The time derivative of V' can be written, using the techniques of flux surface averaging, as

$$\frac{\partial}{\partial t} V'(\psi, t) = -\left(V'\left\langle\frac{\partial \psi}{\partial t}\right\rangle\right)', \tag{15}$$

where the time derivative on the left-hand side is taken at fixed ψ and the time derivative on the right-hand side is taken at fixed (R, Z). In cases involving a constant plasma boundary, the poloidal flux surfaces do not change rapidly in time. Hence, the time rates of change of V' and of the other equilibrium shape-dependent quantities are not large, and such quantities can be treated explicitly in advancing the transport equations. Equation (15) can then be combined with Eqs. (8) and (9) to obtain the following equations:

$$\frac{\partial n}{\partial t} = \frac{n}{V'}\left(V'\left\langle\frac{\partial \psi}{\partial t}\right\rangle\right)' + \frac{1}{V'}(n'V'\langle DR^2B_p{}^2\rangle)' + \langle S_{\text{inj}}\rangle + \langle S_{\text{fuel}}\rangle, \tag{16}$$

$$\begin{aligned}\frac{\partial p}{\partial t} = {} & \frac{5}{3}\frac{p}{V'}\left(V'\left\langle\frac{\partial \psi}{\partial t}\right\rangle\right)' + \frac{1}{V'^{5/3}}\left(pV'^{5/3}\frac{n'}{n}\langle DR^2B_p{}^2\rangle\right)' \\ & + \frac{2}{3}p\left(\frac{n'}{n}\langle DR^2B_p{}^2\rangle\right)' + \frac{2}{3}\frac{1}{V'}\left[\left(\frac{p}{n}\right)' nV'\langle \chi R^2B_p{}^2\rangle\right]' \\ & + \frac{2}{3}(\langle \eta J_\phi{}^2\rangle + \langle H_\alpha\rangle + \langle H_{\text{inj}}\rangle),\end{aligned} \tag{17}$$

where $\partial n/\partial t$ and $\partial p/\partial t$ are taken at fixed ψ and $\partial\psi/\partial t$ is taken at fixed (R, Z). It is possible to advance Eqs. (16) and (17) implicitly one or several time steps, before recalculating the equilibrium, by treating all specifically geometric quantities, i.e., those depending only on flux surface shapes, as explicit terms determined by the most recent equilibrium.

In compressional studies the plasma size, shape, and location may be changing sufficiently fast that the rates of change of V' and the other geometric quantities are significant. Such quantities must then be treated implicitly. Equations (8) and (9) are best used for such problems since the evaluation of $\langle\partial\psi/\partial t\rangle$, in Eqs. (16) and (17),

on a moving coordinate grid presents difficulties. Any approach which treats the geometric terms implicitly leads to a predictor–corrector scheme requiring at least two equilibrium evaluations for each time step.

We have developed such a procedure which consists of two nested, predictor–corrector loops together with an implicit time differencing scheme (Crank–Nicholson). The inner loop advances the equations for a given set of equilibrium conditions and requires very little computer time. The outer loop involves solving the flux-conserved equilibrium at the new time and is, therefore, more time-consuming. Two sets of test values at the new time are retained for each n and p, one set to determine the convergence of each predictor–corrector. Consider a time step $i \rightarrow i + 1$ and let superscripts j and k denote the predictor–corrector iterations for the inner and outer loops, respectively. Then the time-stepping procedure is as follows (see Fig. 3):

(a) Initialize all quantities, including predictor–corrector test values $n_{\text{in}}^{(0)}$, $p_{\text{in}}^{(0)}$, $n_{\text{out}}^{(0)}$, and $p_{\text{out}}^{(0)}$, to the initial values at time step i.

(b) Obtain n_{i+1} by advancing Eq. (8) implicitly, using a tridiagonal matrix. Because p does not appear, Eq. (8) can be advanced independent of Eq. (9). Use all

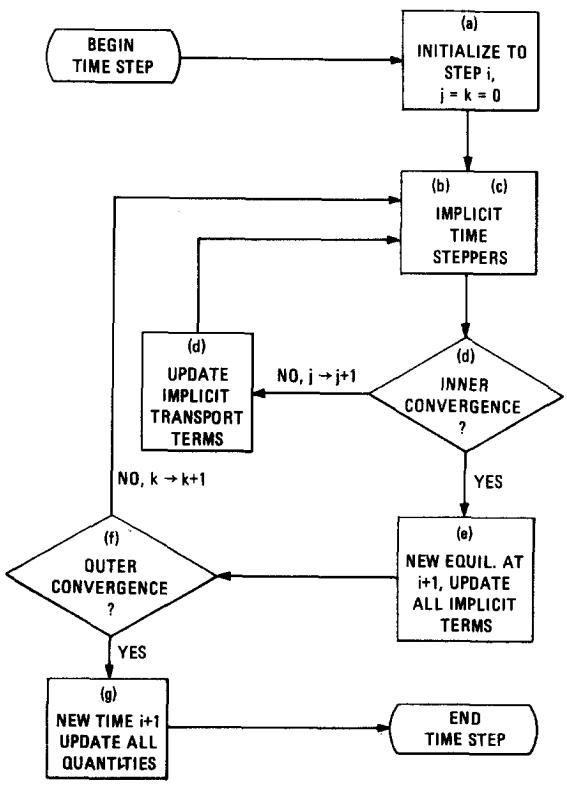

FIG. 3. Flowchart of the transport time advancement numerical procedure described in Section 3.

available quantities at time $i + 1$ in implicit terms and quantities at time i in explicit terms.

(c) Obtain p_{i+1} by advancing Eq. (9) implicitly, using a tridiagonal matrix. Use n_{i+1} obtained in step (b) to advance Eq. (9) independent of Eq. (8). As in step (b), implicit terms contain quantities at time $i + 1$ and explicit terms at time i.

(d) Compare n_{i+1}, p_{i+1}, to $n_{\text{in}}^{(j)}$, $p_{\text{in}}^{(j)}$. If converged, continue to step (e). Otherwise, set $n_{\text{in}}^{(j+1)}$, $p_{\text{in}}^{(j+1)}$ equal to n_{i+1}, p_{i+1}; use n_{i+1}, p_{i+1} to obtain appropriate quantities at time $i + 1$ for use in implicit parts of Eqs. (8) and (9) and return to step (b).

(e) Calculate the equilibrium and all other quantities at time $i + 1$ by using n_{i+1}, p_{i+1}.

(f) Compare n_{i+1}, p_{i+1} to $n_{\text{out}}^{(k)}$, $p_{\text{out}}^{(k)}$. If converged, proceed to step (g). Otherwise, set $n_{\text{out}}^{(k+1)}$, $p_{\text{out}}^{(k+1)}$ equal to n_{i+1}, p_{i+1} and return to step (b). The difference between steps (d) and (f) is that in (f) all quantities, including those which depend only on the equilibrium, are updated to time $i + 1$ while in step (d) equilibrium quantities are not altered.

(g) The time step is completed with both predictor–correctors converged. Set all quantities to the values at time $i + 1$ and proceed to the next time step.

Given the simple transport model used here, very little computer time is required to carry out steps (a)–(d) of the above procedure. The residual in the inner predictor–corrector loop can, therefore, be made quite small. The equilibrium evaluation in step (e) involves most of the computing time in the procedure. Although the equilibrium evaluation occurs in the outer predictor–corrector loop, the computational time increases less than linearly with the number of iterations in the loop because successive iterations result in improved initial guesses for the equilibrium. For example, we find that the above procedure with three iterations in the outer predictor–corrector loop typically requires only twice as much computer time as the first iteration alone. The overall computing time required in plasma simulations using the above procedure depends upon the size of the time step. We have found that, as long as the equilibrium procedure converges, the time required to make a calculation decreases with increasing time-step size. Also, we have found for several test cases that the results are independent of the time-step size as long as all convergence criteria are met.

In order to speed up the calculations when the plasma cross-sectional boundary is fixed, two changes may be made in the above procedure. Equations (16) and (17) should be used instead of Eqs. (8) and (9) to advance the pressure and density. Then the geometric factors can be treated as explicit terms and the outer predictor–corrector loop (step (f), p_{out}, and n_{out}) can be deleted. Hence, the equilibrium is evaluated just once at the end of each time step. It is also possible in this method to carry out several transport time steps before evaluating the new equilibrium and geometric factors in step (e). We have found this modified procedure for fixed plasma boundaries to run approximately twice as fast as the compressional procedure (with three outer

iterations) for cases of constant plasma cross section. In these cases the physical results of the two procedures were in agreement.

The compressional procedure converges for both n and p to 10^{-5} in 5–15 steps on the inner productor–corrector loop. Convergence to 3×10^{-3} for both n and p is typically achieved in three steps on the outer loop. These rates of convergence apply to time-step sizes chosen to give changes of 20% in p and to grid sizes of 31 points in ψ. Because the subsequent equilibria change mildly, the SOR approach to solve for ψ is efficient. Convergence for the modified noncompressional procedure is comparable to that for the inner predictor–corrector loop of the compressional procedure.

3.5. *Numerical Procedures: Summary*

In summary we note that the procedures just described ensure numerical convergence in all physical variables for the one-dimensional and two-dimensional parts of the problem. The geometric coefficients obtained from the equilibrium are used in the implicit advancement of the transport equations only after the 2-D equilibrium calculations have converged for given $p(\psi)$, $q(\psi)$, $\psi_{\text{edge}} - \psi_0$, $F(\psi_{\text{edge}})$, and plasma cross section.

It should be emphasized that adding flux diffusion or more sophisticated transport to the model would have no effect on either the equilibrium procedure or its coupling to the transport. Only the details of the transport time stepping would be altered.

4. Results

4.1. *Neutral Injection to Ignition*

As an example of a case in which the plasma boundary remains nearly fixed we consider the heating of a low-β prototypical reactor plasma to ignition by neutral injection with simultaneous fueling of the plasma. The particle fueling was assumed to penetrate 25 cm into the plasma, which had a minor radius of 125 cm. The fueling rate was chosen to raise the average electron density from $\bar{n}_0 \simeq 5.0 \times 10^{13}$ cm^{-3} to $\bar{n}_0 \simeq 1.5 \times 10^{14}$ cm^{-3} in approximately 5 sec. The FREYA Monte Carlo neutral beam package [22] was used to inject a deuterium beam into a D–T plasma. A 120-keV neutral beam of about 65-MW power was injected horizontally at an angle of 15° from perpendicular with respect to the toroidal direction. Figure 4 shows the evolution of $p'(\psi)$ and $FF'(\psi)$ with time. Figure 5 shows the time evolution of the electron density, the temperature, the injection heating, and the nuclear alpha heating profiles. Figure 6 the average temperature, and the total injection and nuclear alpha heating powers. The profiles in Figs. 4 and 5 are shown for times $t = 0$, 2.09, and 5.29 sec. Plasma ignition occurs at about 5 sec, at which time the nuclear alpha heating exceeds the injection power. In this calculation F_{edge} was kept constant. The variation in the plasma minor radius a was less than 0.5%.

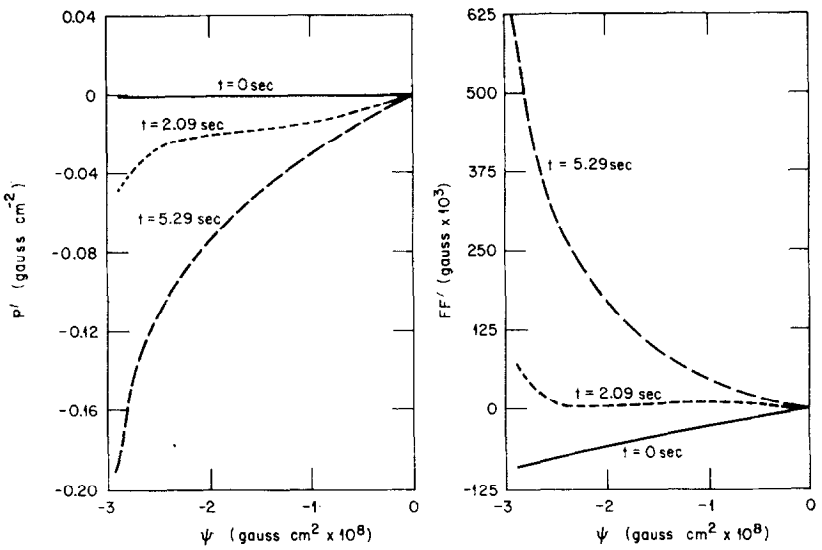

FIG. 4. Evolution of the $p'(\psi)$ and $FF'(\psi)$ profiles in time for the neutral injection calculation described in Section 4. The solid curves plot the initial profiles, the dotted curves correspond to a time of 2.09 sec, and the dashed curves show the profiles at 5.29 sec. Note how FF' mirrors p' as F changes to conserve flux during the evolution of the plasma.

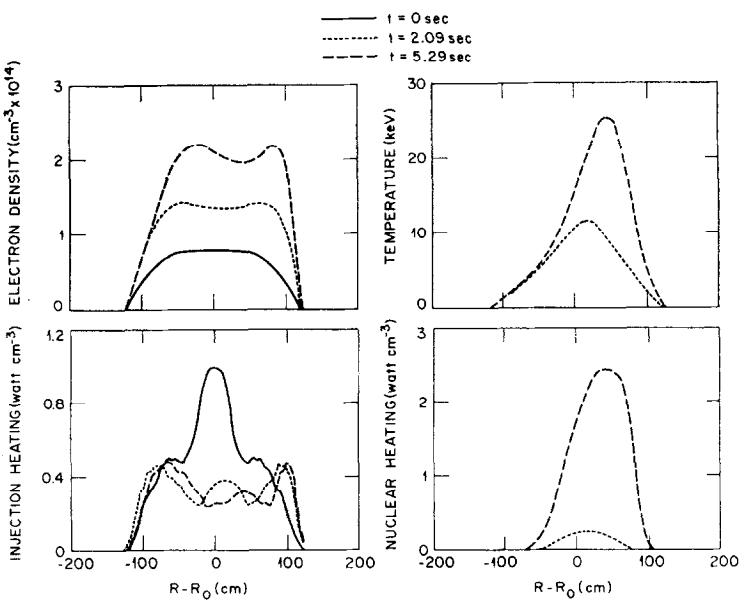

FIG. 5. Evolution of the electron density, temperature, neutral injection heating, and nuclear alpha heating profiles for the neutral injection calculation described in Section 4. The solid curves plot the initial profiles, the dotted curves correspond to a time of 2.09 sec, and the dashed curves show the profiles at 5.29 sec. As the density increases, few 120 keV neutrals penetrate to the plasma center. However, the resulting decrease in neutral heating at the center is offset by increased nuclear alpha heating, and the plasma ignites.

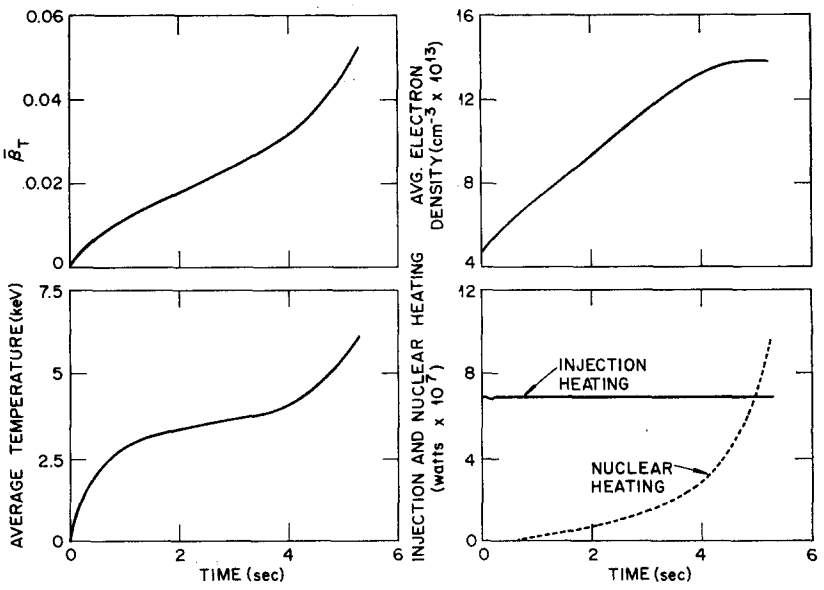

FIG. 6. Time evolution of $\bar{\beta}_T$, the average electron density, the average temperature, and the total injection and nuclear alpha heating powers for the neutral injection calculation described in Section 4. In the final plot, the solid curve represents the injection heating, and the dotted curve represents the nuclear alpha heating.

4.2. *Compression in Major and Minor Radius*

As a natural example, in order to obtain a plasma of small aspect ratio (A), we consider compression along the major and minor radii by prescribing the plasma boundary cross section as a function of time. During the compression we assume $F_{\text{edge}} = \text{constant}$. For compressions which are rapid compared to the resistive skin time, both toroidal and poloidal magnetic flux are well conserved; i.e., $q(\psi)$ and $\psi_{\text{edge}} - \psi_0$ are fixed. Assuming that $B_\phi \propto 1/R$ [i.e., $F(\psi_{\text{edge}}) = \text{constant}$], Furth and Yoshikawa [24] have shown that, for plasmas of fixed cross-sectional shape in the limit of large aspect ratios, toroidal magnetic flux conservation implies that the plasma minor radius must vary as

$$a \propto R^{1/2} \tag{18}$$

during the compression. Using Eq. (18) and the above assumptions, they derive a set of compressional scaling laws for the parameters characterizing the plasma; e.g., the plasma current satisfies $I_p \propto 1/R$.

As the plasma is compressed toward small aspect ratios, the assumption Eq. (18) and the resulting compressional scaling laws may require modification. In order to test this, we carried out compressional simulations in which

$$a \propto R^p \tag{19}$$

with several values of p to study the variation of $(\psi_{edge} - \psi_0)$ with compression. We considered the compression of an elongated D-shaped plasma with a fixed elongation and triangularity. The initial values of the major and minor radii were taken to be $R_0 = 240$ cm and $a = 80$ cm, respectively. The final values were chosen to satisfy Eq. (19) and $R - a = 20$ cm (see Fig. 7). For the Furth–Yoshikawa scaling law ($p = 0.5$), the final values are $R = 60$ cm and $a = 40$ cm (i.e., $A = 3 \rightarrow A = 1.5$). The compression in the major radius R was taken to be linear in time, and the duration of the compression was $\tau_c = 0.2$ sec (the initial energy confinement time was $\tau_E = 0.3$ sec). A hydrogen plasma was assumed so that no nuclear heating would be present. In addition, the injection and particle fueling source terms were turned off.

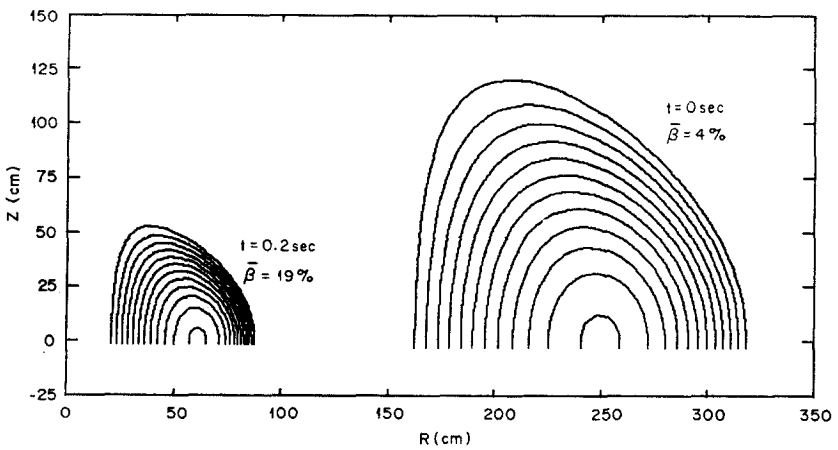

FIG. 7. Flux surfaces (of constant ψ) for the initial and final states for the $\tau_c = 0.2$ sec, $p = 0.57$ compressional calculation described in Section 4. The larger (outer) set of contours shows the low (~4 %) β initial state, and the smaller (inner) set of contours shows the high (~19 %) β compressed final state.

Figure 8 shows the variation of $\psi_{edge} - \psi_0$ with time, for fixed $F(\psi_{edge})$ and $q(\psi)$, for cases having $p = 0.5$, 0.54, 0.57, and 0.6. It is seen that the power p required to maintain $\psi_{edge} - \psi_0$ constant changes with the aspect ratio of the plasma. Early in the compression, $p = 0.54$ best conserves $\psi_{edge} - \psi_0$, and at the end of the compression $p = 0.6$ conserves $\psi_{edge} - \psi_0$. The initial and final values of $\psi_{edge} - \psi_0$ are most nearly equal for $p = 0.57$. Note that if $\psi_{edge} - \psi_0$ were fixed, either a or $F(\psi_{edge})$ would then change in these calculations.

Figure 9 shows the evolution with time of the plasma current profiles during the $p = 0.57$ compression. Note that the current profile becomes somewhat hollow as the plasma is compressed, although the $q(\psi)$ profile remains unchanged and monotonic between 1.0 and 3.0. The total plasma current is found to increase by a factor above 6, which differs significantly from the scaling of $I_p \propto 1/R$. Additional study, presently under way, is needed to understand in detail the effects of plasma boundary shape, small aspect ratios, and $q(\psi)$ profiles on the compressional scaling laws.

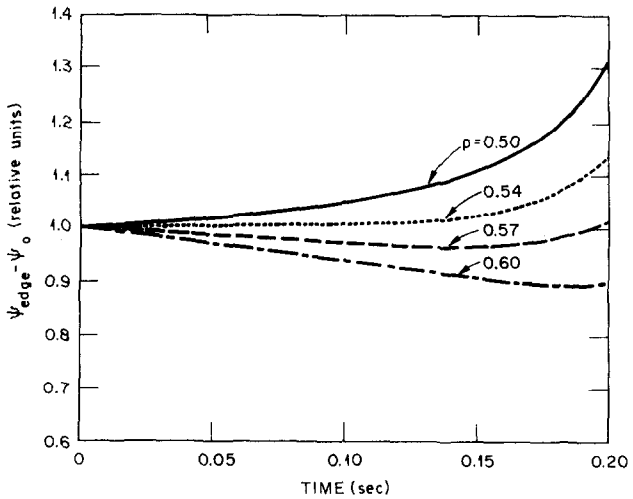

FIG. 8. Time evolution of $\psi_{edge} - \psi_0$ for several $\tau_c = 0.2$ sec compressional calculations as described in Section 4. The solid curve corresponds to the Furth–Yoshikawa scaling of $p = 0.5$ in Eq. (25). The dotted curve, the dashed curve, and the dot-dashed curve plot cases having $p = 0.54$, 0.57, and 0.6, respectively. Note that the power law required to satisfy poloidal flux conservation ($\psi_{edge} - \psi_0$ constant) varies as the aspect ratio decreases (time increases).

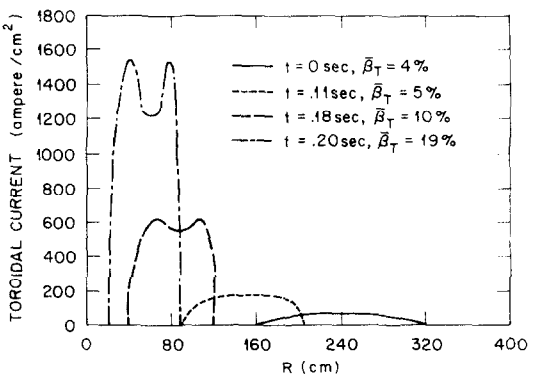

FIG. 9. Evolution of the toroidal current profile for the $\tau_c = 0.2$ sec, $p = 0.57$ compressional calculation described in Section 4. The solid, dotted, dashed, and dot-dashed curves correspond to times of 0, 0.11, 0.18, and 0.20 sec and to β_T of 4, 5, 10, and 19%, respectively.

5. SUMMARY

The model and associated procedures discussed in this work provide a method for studying the time evolution of MHD equilibria subject to various particle and energy source terms. The numerical results obtained by these procedures satisfy satisfactory convergence criteria as well as consistency between the one-dimensional and two-

dimensional parts of the problem. Through the use of a fixed boundary equilibrium routine, it is possible to prescribe the evolution of the plasma boundary to permit us to treat cases in which the plasma cross section changes significantly and in which precise plasma positioning and shaping are required, without the necessity of using external fields and coils. The required external fields can then be calculated from the evolving MHD equilibrium data determined here [14]. This data can also be used as input in high-β MHD stability studies.

Applications of the model presented here included the neutral beam heating of a prototypical reactor plasma to ignition and a compressional heating case designed to explore modifications to the Furth–Yoshikawa scaling law at small aspect ratio.

ACKNOWLEDGMENTS

The authors wish to acknowledge R. A. Dory, R. H. Fowler, W. A. Houlberg, J. Smith, and D. J. Strickler for fruitful discussions and suggestions.

This work was funded by the Fusion Energy Division at the Oak Ridge National Laboratory.

REFERENCES

1. J. F. CLARKE AND D. J. SIGMAR, *Phys. Rev. Lett.* **38** (1977), 70.
2. R. A. DORY AND Y.-K. M. PENG, *Nucl. Fusion* **17** (1977), 21.
3. T. OHKAWA *et al.*, *in* "Plasma Physics and Controlled Nuclear Fusion Research," Vol. I, p. 281, Intern. At. Energy Agency, Vienna, 1975 (paper IAEA-CN-33/A10-1 presented at the 5th Int. Conf. on Plasma Physics and Controlled Nuclear Fusion Research, Tokyo, Japan, 1974).
4. D. M. MEADE *et al.*, *in* "Plasma Physics and Controlled Nuclear Fusion Research," Vol. I, p. 605, Intern. At. Energy Agency, Vienna, 1975 (paper IAEA-CN-33/A15-4 presented at the 5th Int. Conf. on Plasma Physics and Controlled Nuclear Fusion Research, Tokyo, Japan, 1974).
5. D. W. SWAIN, Y.-K. M. PENG, M. MURAKAMI, AND L. A. BERRY, *Bull. Amer. Phys. Soc.* **22** (1977), 1158.
6. Y-P. PAO, *Phys. Fluids* **19** (1976), 1177.
7. H. GRAD AND J. HOGAN, *Phys. Rev. Lett.* **24** (1970), 1337.
8. J. T. HOGAN, "The Accessibility of High-β Tokamak States," ORNL/TM-6049, May 1978.
9. J. T. HOGAN, "Ideal MHD Stability of Tokamak Equilibria," ORNL/TM-6273, May 1978.
10. S. C. JARDIN, S. P. HIRSHMAN, AND J. L. JOHNSON, "Two Dimensional Transport of Tokamak Plasmas," paper presented at the Annual Controlled Fusion Theory Conference (Sherwood Theory Meeting, ORNL, Gatlinburg, Tenn. 1978).
11. R. N. BYRNE AND H. H. KLEIN, *J. Comput. Phys.* **26** (1978), 352.
12. B. CARRERAS, H. R. HICKS, AND B. V. WADDELL, "Tearing Mode Activity for Hollow Current Profiles," ORNL/TM-6570, October 1978.
13. Y-K. M. PENG, R. A. DORY, D. B. NELSON, AND R. O. SAYER, *Phys. Fluids* **21** (1978), 467.
14. Y-K. M. PENG, R. A. DORY, AND D. J. STRICKLER, to be published as an ORNL/TM.
15. M. MURAKAMI *et al.*, "Plasma Confinement and Impurity Flow Reversal Experiments in the ISX-A Tokamak," paper IAEA-CN-37/N-4 presented at the 7th Int. Conf. on Plasma Physics and Controlled Nublear Fusion Research, Innsbruck, Austria, 1978; to be published in proceedings.

16. H. EUBANK *et al.*, "PLT Neutral Beam Heating Results," paper IAEA-CN-37/C-3 presented at the 7th Int. Conf. on Plasma Physics and Controlled Nuclear Fusion Research, Innsbruck, Austria, 1978; to be published in proceedings.
17. J. D. CALLEN AND R. A. DORY, *Phys. Fluids* **15** (1972), 1523.
18. H. GRAD, P. N. HU, AND D. C. STEVENS, "Adiabatic Evolution of Plasma Equilibrium," Courant Institute of Mathematical Sciences, MF-83, COO-3077-92, 1975.
19. F. L. HINTON AND R. D. HAZELTINE, *Rev. Med. Phys.* **48** (1976), 239.
20. L. A. BERRY *et al.*, *in* "Plasma Physics and Controlled Nuclear Fusion Research," Vol. I, p. 49, Intern. At. Energy Agency, Vienna, 1977 (paper IAEA-CN-35/A4-1 presented at the 6th Int. Conf. on Plasma Physics and Controlled Nuclear Fusion Research, Berchtesgaden, Germany, 1976).
21. W. A. FOWLER, G. R. CAUGHLAN, AND B. A. ZIMMERMAN, *Ann. Rev. Astron. Astrophys.* **13** (1975), 69.
22. G. G. LISTER, D. E. POST, AND R. GOLDSTON, "Computer Simulation of Neutral Beam Injection into Tokamaks Using Monte Carlo Techniques," paper presented at the 3rd Symposium on Plasma Heating in Toroidal Devices, Varenna, Italy, 1976; R. H. FOWLER, J. A. HOLMES, AND J. A. ROME," NFREYA—A Monte Carlo Beam Deposition Code for Noncircular Tokamak Plasmas," ORNL/TM-6845, May 1979.
23. D. J. STRICKLER (Oak Ridge National Laboratory), private communication, 1978.
24. H. P. FURTH AND S. YOSHIKAWA, *Phys. Fluids* **13** (1970), 2593.